Mine Water and the Environment (2022) 41:237–251
https://doi.org/10.1007/s10230-022-00847-w

TECHNICAL ARTICLE

Using sUAS for the Development and Validation of Surface Water Quality Models in Optically Deep Mine Waters

Brandon K. Holzbauer-Schweitzer[1] · **Robert W. Nairn**[2]

Received: 23 April 2021 / Accepted: 18 January 2022 / Published online: 7 February 2022

Abstract

This study demonstrated novel remote monitoring techniques for mining-impacted surface waters using spectral data from two different platforms (multispectral sUAS and handheld hyperspectral sensors) and the feasibility of using sUAS-derived multispectral imagery to estimate in-situ metal concentrations in two passive mine drainage treatment systems. Strong linear relationships (e.g. $R^2_{adj.} > 0.74$) were found between multispectral reflectance and various in-situ constituent concentrations (e.g. Fe, Li, Mn, Pb, and Zn). Developed ordinary least squares (OLS) models estimated mean metal concentrations within 1% of the observed value and a 70% confidence interval. Validation at a separate site treating waters of a different geologic origin allowed us to assess the models' site-specificity. Validation of some models was not possible within this study's statistical constraints (e.g. ± 25% of the observed in-situ value). However, two models were validated and when the linear relationships were examined with site-specific spectra (i.e. sUAS-derived multispectral imagery), significant improvements to the models were observed. Employing hyperspectral remote sensing techniques yielded a novel identification procedure for optically shallow waters. This exponential relationship (e.g. $R^2 = 0.73$) evaluates the feasibility of using remote sensing technologies to assess water quality before any model development efforts. A tool capable of identifying remote sensing interferences will be crucial for the future of environmental remote sensing. Using sUAS to estimate in-situ water quality provides a new way to monitor passive mine water treatment systems, potentially advancing the efficiency and cost-effectiveness of monitoring and altering traditional environmental remote sensing strategies.

Keywords Regression · Remote sensing · Multispectral · Hyperspectral · Optical depth

Introduction

Monitoring Mining Impacted Environments

All mining stages (e.g. exploration, design and planning, construction, production, closure, and reclamation) influence landscapes worldwide (Ali et al. 2017; Bebbington et al. 2018; Buczyńska 2020; Tiwari and De Maio 2018; Werner et al. 2020). However, mineral and fuel extraction is expected to continue for the foreseeable future (Martins et al. 2020), with an ever-increasing need for sustainable reclamation practices based on sound science. Reclamation of a mining-impacted landscape is not a rapid process and can require in-situ data across vast spatial and temporal scales (Werner et al. 2020). Unfortunately, evaluating the success of mining reclamation projects is often overlooked due to time, person-hours, monetary and logistical constraints. Specifically, these attempts often fail to capture the spatial and temporal variation of complex inland water bodies (Becker et al. 2019; Biber 2013; Holl 2002).

Therefore, advancements in environmental monitoring strategies and data collection technologies are critical. One such approach includes incorporating remote sensing data, specifically small unoccupied aerial system (sUAS)-derived information (e.g. multispectral reflectance) into traditional environmental monitoring and reclamation projects (Becker et al. 2019; Shi et al. 2019). As electromagnetic (EM) energy passes through Earth's atmosphere and encounters an object,

✉ Brandon K. Holzbauer-Schweitzer
Bholzbauersch10@gmail.com

Robert W. Nairn
nairn@ou.edu

[1] Linkan Engineering, 400 Corporate Circle, Suite H, Golden, CO, USA

[2] Center for Restoration of Ecosystems and Watersheds, University of Oklahoma, 202 West Boyd Street, Room 334, Norman, OK, USA

several interactions occur (e.g. reflection, transmission, absorption, and scattering) between the photons and particles within the medium. In a shallow and transparent water body, photons interact with the bottom substrate, altering and interfering with the expected energy signal [i.e. optically shallow waters (OSWs)] (Albert and Gege 2006; Cannizzaro and Carder 2006; Salama et al. 2009). In other words, if substrate is visible through a water column, multispectral sensors will detect it, causing the reflected EM energy signature to be modified and making the development of statistical models a complex task. Conversely, if optically active constituents (OACs) (e.g. particulate Fe, chlorophyll-a, total suspended solids) are present in elevated concentrations and hide the bottom substrate, even in physically shallow surface waters, visible (VIS) EM energy will decay at an exponential rate, and interactions with the substrate will be nominal (Cannizzaro and Carder 2006; Zeng et al. 2017). These aspects of optically deep waters (ODWs) allow for the development of relationships between reflected spectral energy and in-situ metal concentrations.

Terrestrial applications of sUAS technologies have been effective in several mining phases (Lee and Choi 2016; Park and Choi 2020; Ren et al. 2019). Cress et al. (2015) established a roadmap for performing geological surveys in the conterminous United States. Lee and Choi (2016) demonstrated how sUAS could produce high-resolution topographic surveys. Fang et al. (2019) used hyperspectral data and regression techniques to map Fe accumulation in exposed soil at a reclamation site. Several authors have demonstrated how spectral measurements in water bodies can estimate concentrations of various traditional OACs (e.g. chlorophyll-a, total suspended solids, and turbidity) (Arango and Nairn 2020; Cannizzaro and Carder 2006; Dekker et al. 1996; Lim and Choi 2015; Matthews and Odermatt 2015; Su 2017). Limited research has examined how sUAS-derived multispectral reflectance can describe an aquatic environment affected by mining activities and some recent efforts have successfully demonstrated this using more advanced (i.e. significantly more spectral bands) hyperspectral sensors (Flores et al. 2021).

However, sUAS have limitations (Gholizadeh et al. 2016; Whitehead and Hugenholtz 2014; Zhang et al. 2019; Zeng et al. 2017). Some regulatory and technical constraints of sUAS include flight altitude limitations, line of sight requirements, short flight times, and limited payload capabilities, along with concerns about GPS and sensor accuracy (FAA 2016; Ren et al. 2019; Watts et al. 2012). From a scientific perspective, the lack of a standardized operating procedure for collecting environmental data and applying it to reclamation monitoring has been a considerable limitation (Buters et al. 2019; Shi et al. 2019). Many authors have also commented on the difficulty of developing empirical models, referencing the need to derive site-specific inherent optical properties (IOPs) and manage complex signals from turbid water, bottom reflectance, and mixed pixels (Cannizzaro and Carder 2006; Gholizadeh et al. 2016; Lee et al. 1998; Lee and Carder 2002; Palmer et al. 2015; Salama et al. 2009; Su 2017; Voss et al. 2003). Thus, the need to establish robust datasets for non-traditional water quality parameters (i.e. metals) and explore the applications' potential is apparent.

Hypotheses and Purpose

Therefore, the two hypotheses of this study were: (1) combining various bands or band transformations from sUAS-derived multispectral imagery and in-situ surface-water quality will allow for the development of statistical models capable of predicting metal concentrations in mining-impacted surface waters, and (2) water quality models will remain valid when developed and tested in waters of different geologic origin. First, the feasibility of using sUAS-derived multispectral imagery to estimate in-situ metal concentrations in lead–zinc mine drainage was examined. Then, models were assessed for accuracy and statistical validity in coal mine drainage of a different geologic origins. Finally, a method to remotely evaluate a waterbody's potential for these applications of sUAS technologies was developed.

Materials and Methods

Study Site Descriptions

The study locations for this study were two mine water passive treatment systems (PTS). The Mayer Ranch PTS (MRPTS) and the Hartshorne PTS (HPTS) served as the test and validation study sites, respectively. MRPTS is located within the Tar Creek Superfund Site, in the Oklahoma portion of the 6475 km^2 tri-state lead–zinc mining district (Fig. 1a–d). Nearly 460 million tons of lead and zinc ore were produced from the mid-1800s to 1970, leaving a derelict landscape contaminated with mining-related hazards, such as mining waste and contaminated water resources (ODEQ 2017). MRPTS was designed and implemented to address nearly 1000 L/min of net-alkaline artesian-flowing mine water contaminated with elevated levels of As, Cd, Fe, Ni, Pb, Zn, and SO_4^{2-} (Nairn et al. 2020). Operated in two parallel treatment trains, the ten-cell PTS has effectively treated net alkaline ferruginous mine drainage since 2008 (Nairn et al. 2010). HPTS is located within the Oklahoma portion of the 87,500 km^2 Arkoma Basin coalfields (Fig. 1a, b, e, and f). Specifically, HPTS is located at Rock Island Improvement mine #7, which from 1907 to 1931 produced ≈ 500,000 t of Lower Hartshorne coal from more than 100 m underground (Friedman 1996; USGS 1996). HPTS was designed to treat about 40 L/min of net-acidic

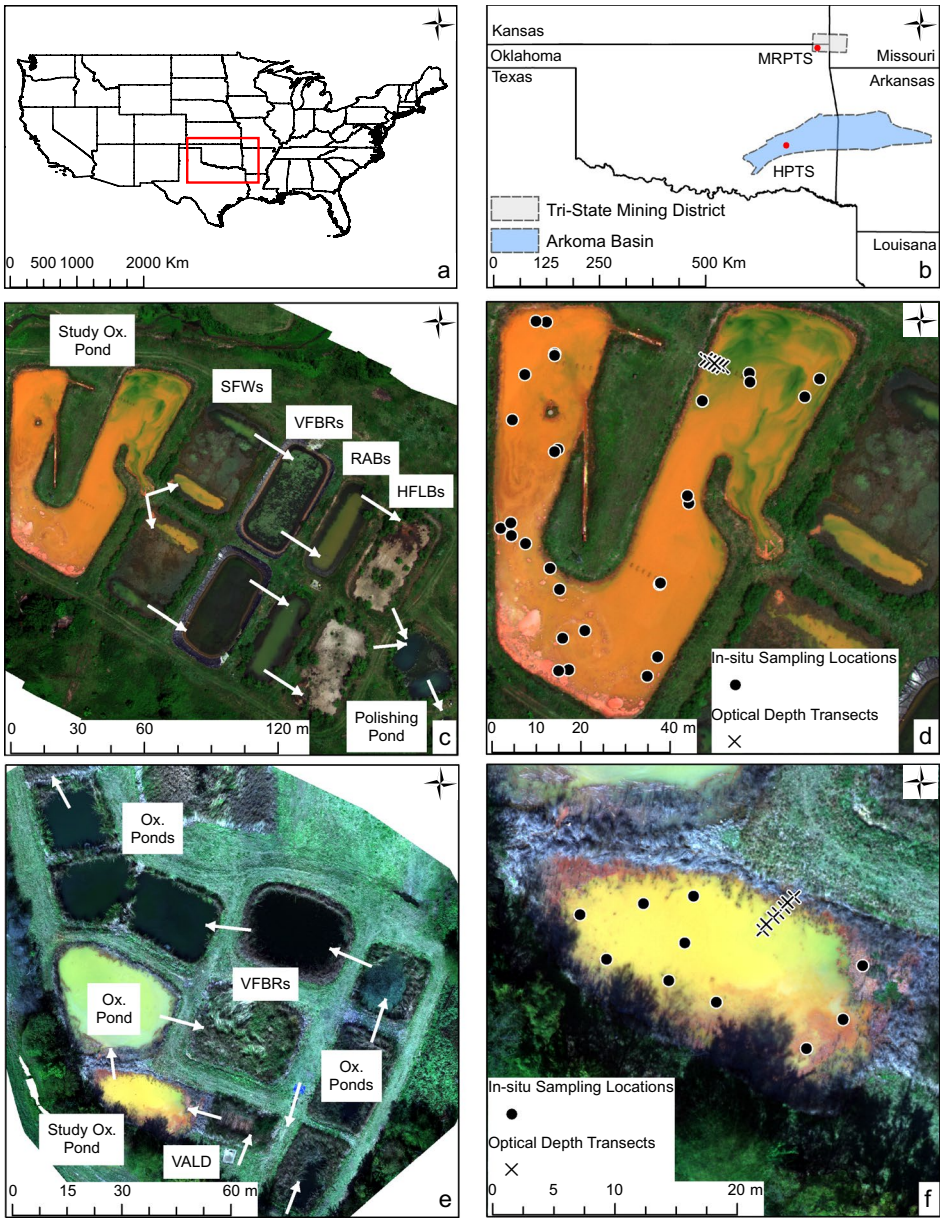

Fig. 1 **a** The study location within the United States of America; **b** the general location of Mayer Ranch passive treatment system (MRPTS) and Hartshorne passive treatment system (HPTS) within the state of Oklahoma; **c**: MRPTS' process units: oxidation (Ox.) pond, surface flow wetlands (SFWs), vertical flow bioreactors (VFBRs), re-aeration basins (RABs), and horizontal-flow limestone beds (HFLBs), with the general flow path indicated by white arrows; **d**: locations where in-situ samples were collected and hyperspectral profiles were completed; **e**: HPTS' groups of process units (vertical anoxic limestone drain (VALD), Ox. pond(s), and VFBRs, with the general flow path indicated by white arrows; and **f**: the locations where in-situ samples were collected and hyperspectral profiles were generated

artesian-flowing mine drainage contaminated with elevated levels of Fe, Mn, and SO_4^{2-}. Since 2007, the six-cell PTS has consistently removed trace metals and mineral acidity and discharges a net alkaline effluent (LaBar and Nairn 2009).

Both PTS have an initial oxidative unit near the beginning of the treatment trains which were of focus in this study. It was the similarities concerning optical depth (OD), system design and age, influent water quality, and dominant optical properties that made the two oxidative units ideal candidates for testing water quality models developed using visible/near-infrared (NIR) EM energy. One important note is that each system's source waters differed in geologic origin and the targeted mining products (e.g., Pb and Zn at MRPTS; coal at HPTS). Mine drainage at MRPTS was produced from Mississippian carbonate host rocks (i.e., limestone and dolostone) with ores dominated by galena and sphalerite (McKnight and Fischer 1970). In contrast, mine drainage at HPTS stems primarily from the Hartshorne coal and associated quartzose sandstone with interbedded shales (Trumbull 1957). Due to the geologic host rock present at MRPTS and the incorporation of a vertical anoxic limestone drain (VALD; alkalinity production via anoxic limestone dissolution and bicarbonate generation; Fig. 1e) at HPTS, influent waters at both sites were net alkaline with elevated metal concentrations. Even though the studied waters were similar in nature, assessing the validity of sUAS-derived models in waters sourced from different geologic origins remains an unexplored scientific question.

In-situ Data Collection

Spectral Measurements

Before collecting spectral data, instruments were field-calibrated. An Analytical Spectral Devices FieldSpec3 was optimized and standardized with a white calibrated reflectance panel to reflect 95–99% of EM energy. This calibration procedure was completed every 10 min or when illumination conditions (e.g. cloud cover) changed during data collection. The data generated at each wavelength represents the average of ten samples taken in 0.1 s increments. The hyperspectral (i.e. 350–2500 nm) profiles were collected with respect to nadir (i.e. perpendicular to the water surface). Measurements were collected ≈ 1 m above the water surface at 1 m horizontal increments starting at the water's edge, or 0 m (Fig. 1d and e). Each set of ten measurements was collected five times, averaged, and post-processed to spectral reflectance using Analytical Spectral Devices ViewSpec Pro V6.2 processing software.

Calibration of the MicaSense RedEdge multispectral sensor (RedEdge sensor) required pre- and post-flight reflectance information from the same calibrated reflectance panel. To account for changes in solar conditions throughout the flight, the processing software (Pix4DMapper) used both the pre- and post-flight sets of images. The sensor was fixed via a gimbal to an Aerial Technologies International (ATI) vertical take-off and landing AgBot quadcopter. This vertical take-off and landing sUAS simultaneously collected imagery in five discrete spectral bands (i.e. blue, green, red, red-edge, and NIR) with center points at 475, 560, 668, 717, and 840 nm, respectively. At both PTS, the sUAS-derived multispectral imagery was collected autonomously within ± 2 h of local solar noon. Use of Mission Planner V.1.3.37 software allowed for the development of autonomous missions. Parameters at each PTS included operations at 6 m/s, 60 m above ground level, with at least 75% image side and overlap. With these parameters, the raw uncompressed 16-bit digital number imagery was transformed to high-resolution (i.e. < 10 cm per pixel) 32-bit spectral reflectance orthomosaics using the processing software. If remote sensing interferences affected either multispectral spectral dataset, outliers were identified and removed using the interquartile range of each multispectral band.

Water Quality

The model development dataset consisted of 30 in-situ surface water grab samples collected from MRPTS during the summer of 2019. The use of a fully extended 3.6 m swing-arm sampling pole allowed us to collect 20 samples from the pond's shore below the surface (< 1 m) or until the 1 L HDPE bottle was no longer visible. Ten additional samples were collected similarly from the center of the pond via a canoe. The validation data set was comprised of ten in-situ surface water grab samples from HPTS during the fall of 2020. Samples at HPTS were collected in the same manner as the shoreline samples at MRPTS. At every sampling location, GPS coordinates, along with samples for total and dissolved (< 0.45 µm) metal analyses, were collected. Samples were filtered in the field immediately after collection for dissolved metals analyses using a 0.45-µm inline disposable groundwater filter capsule and hand pump. Samples for both total and dissolved metals analyses were pH adjusted with trace-metal grade nitric acid to a pH < 2 and stored out of sunlight at 4 °C until analyses could be completed. Total and dissolved constituents (i.e. Ag, Al, As, Ba, Ca, Cd, Co, Cr, Cu, Fe, K, Li, Mg, Mn, Na, Ni, Pb, S, Se, Si, and Zn) were analyzed following EPA approved methods, i.e. EPA 3015A (1994) and EPA 6010C (2000), allowing for calculation of the particulate metal fraction (i.e. total minus dissolved). The analytical instrumentation used included a CEM microwave accelerated reaction system with a MarsXpress temperature control system and a Varian Vista-PRO simultaneous axial inductively coupled plasma-optical emission spectrometer (ICP-OES), following US EPA Methods 3015A and 6010C, respectively. In-field analytical quality assurance and quality control protocols included collection of field blanks (deionized water) and randomly selected field duplicates for every ten samples collected. Laboratory analytical quality assurance and quality control efforts followed US EPA approved quality assurance project plans and quality management plans and included blanks, duplicates, digestion blanks, randomly selected digestion duplicates and known additions, laboratory fortified blanks, randomly selected laboratory duplicates and known additions, and check standards (i.e. 0.001–10, 50, and 100 ppm Varian ICP-OES calibration solution), which comprised greater than 20% of the total samples analyzed for any given sample analysis run. To further characterize the water body while remaining within the desired one hour time window of sUAS flights, total alkalinity (i.e. EPA 310.1 1978), turbidity (i.e. ASTM 2130-B 2017), and multiple physicochemical parameters (e.g. temperature, pH, specific conductance) measurements were collected from the center of the pond at MRPTS. Statistical differences between the two water quality data sets were quantified using Welch's unequal variances *t* test and Tukey–Kramer test in Microsoft Excel. These tests allowed sets of data to be compared without assumptions regarding variance or sample size. Outliers in each water quality dataset were identified and removed using the interquartile range of each water quality parameter.

Examining Optical Depth Influences

After collecting spectral data, Secchi disk depth (SDD) and actual water depth (AD) were measured in transects at equal increments (i.e. 1 m) from the shores of the oxidation ponds (Fig. 1d and e). To minimize the resuspension of substrate and modification of the water column's optical properties, SDD was measured first. AD was then measured by lowering a weighted line into the water column until it contacted the substrate's surface. Assuming that SDD is proportional to OD, an SDD to AD ratio equal to one would result in remote sensing interferences (i.e. bottom substrate). Derivation of the relationship involved using the SDD to AD ratio and reflectance from the center point of the RedEdge sensor red band (668 nm) from both PTS (i.e. OD model). Utilizing the raster calculator in ArcMap V. 10.6.1 to generate a surface demonstrated the ability to identify remote sensing interferences in ODWs (i.e. SDD:AD ≥ 1).

Modelling Surface Water Quality

Overall, the approach used to develop the water quality models followed the empirical method described by Dekker and Donze (1994) and applied by numerous other authors (e.g. Arango and Nairn 2020; Cannizzaro and Carder 2006; Dekker et al. 1996; Lim and Choi 2015; Matthews and Odermatt 2015; Su 2017). This method utilizes derived statistical relationships between measured multispectral reflectance and in-situ water quality. However, we attempted to disprove the Dekker and Donze (1994) statement that "the results have no multitemporal validity," when commenting on the practical limitations of such models.

Candidate water quality models were identified by first performing exploratory ordinary least squares (OLS) regression in ArcMap V. 10.6.1. OLS regression uses the entire dataset to minimize the mean squared error (MSE) of the algorithm. Each exploratory run evaluated every possible combination (≈ 40,000) of one, two, and three input candidate explanatory variables (i.e. untransformed and log-transformed multispectral reflectance bands and band ratios) to develop the OLS models that best explained the dependent variable (e.g. in-situ total and particulate metal concentrations). Relationships among these variables were identified using the correlation coefficient (R), allowing for simple data exploration. Model selection criteria (Table 1) were set to satisfy OLS regression assumptions and produce statistically significant, well-fit, and unbiased surface water quality models.

The OLS tool in ArcMap V. 10.6.1 was used to calculate and evaluate the criteria in Table 1. However, a brief explanation of each metric may assist with interpreting the results of this study. An insignificant Jarque–Bera statistic (p value > 0.01) indicated that the regression residuals (i.e. observed minus predicted value) were normally distributed and the predictions displayed no significant bias. Non-normally distributed residuals suggest that not all explanatory variables were accounted for, nonlinear relationships were being modeled, or outliers significantly affected the models. The Koenker studentized (Breusch-Pagan, or BP) statistic was used to assess the consistency of the relationship between the independent and dependent variables in geographic and data space. In other words, if the relationship (i.e. slope) was similar between the variables at all of the sampling locations (i.e. stationary) and that relationship did not change (i.e. linear to nonlinear) with changes in the magnitude of the explanatory variable (i.e. homoscedasticity), the models were specified correctly (i.e. a key variable was not missing). Moran's I and Getis-Ord Global G (Gi^*) were used to assess spatial autocorrelation and clustering of the raw data and regression residuals. Evidence of significant spatial autocorrelation (p-value > 0.05) further suggests that an explanatory variable was excluded from the model. Clustering was used to identify if any sampling location or region produced consistently higher or lower values (i.e. high-low clusters) that were significant at p-values > 0.05. The joint-F test statistic (Joint-F) provided an assessment of multiple regression model significance (p-value < 0.01) compared to a model with no independent variables (i.e. an intercept only model). Finally, the variance inflation factor (VIF) was a metric describing the redundancy among explanatory variables in the multiple regression model. VIF is the reciprocal of tolerance. Although no explicit rule exists, it has been suggested that VIF > 10 indicates severe collinearity, poor estimation of regression coefficients, and an inflated standard error of regression (Marquardt 1970). All of the statistical metrics and tools described in this paragraph were outputs from the OLS tool or analyzed separately in ArcMap V. 10.6.1 (ESRI 2018).

Models selected for further evaluation outperformed the selection criteria. In these cases, models with the highest adjusted (i.e. number of explanatory variables) coefficient of determination ($R_{adj.}^2$) and lowest Akaike information criterion adjusted for small sample sizes (AICc) were chosen for

Table 1 Exploratory regression model criteria set to satisfy the assumptions of OLS regression in ArcMap V. 10.6.1

Statistical parameter	Selection threshold
$R^2_{adjusted}$	> 0.75
Minimum Jarque–Bera	p-value > 0.01
Minimum Koenker	p-value > 0.01
Minimum Moran's I	p-value > 0.05
Minimum Getis-Ord	p-value > 0.05
Maximum Joint-F	p-value < 0.01
Maximum VIF	< 7.5

testing and validation. Several metrics (e.g. residuals, % difference, MSE, mean absolute error (MAE), along with upper and lower confidence intervals) assessed the validity of the models developed and tested in MRPTS waters at HPTS. Acceptance of the experimental hypotheses required that the models produce predictions of MRPTS metal concentrations within the 75% confidence interval and that the predicted HPTS mean metal concentrations fall within ± 25% of the measured value.

Results and Discussion

In-situ Water Quality

Mean in-pond metal concentrations at MRPTS and HPTS were similar to mining-impacted waters found throughout the tri-state lead–zinc mining district and Arkoma Basin, respectively (Table 2; LaBar and Nairn 2009; Nairn et al. 2010). Some parameters were not detected in either system (e.g. Ag, As, Cr, and Se). Others (e.g. Ba, Ca, K, Mg, Na, and Si) were not considered because of the minimal environmental risk posed at the observed concentrations. Furthermore, some metals (e.g. Cd, Co, and Cu) were quantifiable (i.e. > practical quantitation limit (PQL)) at MRPTS but not at HPTS; thus, they were not considered within the context of this study (Holzbauer-Schweitzer and Nairn 2020). Therefore, the emphasis was placed on in-situ concentrations of particulate Fe and total Li, Mn, Ni, Pb, S, and Zn.

A review of the relationships between water quality parameters revealed that Li, Mn, Ni, Pb, S, and Zn were strongly and collinearly related ($R > 0.90$) at MRPTS. Interestingly, the dominant OAC (i.e. particulate Fe) exhibited no relationship ($R < 0.10$) with the other metals. At HPTS, only the Li, Mn, Ni, and Pb displayed strong collinearity ($R < -0.80$). S exhibited weak relationships ($R < 0.20$) with

Table 2 Observed in-situ multispectral reflectance for each band and water quality for the constituents examined

Parameter	Site	Mean	Median	Min	Max	Var	W-T *p*-value	T-K *p*-value
Reflectance								
Blue	MR	0.040	0.038	0.027	0.079	1.15E-04	6.46E-02	–
	H	0.036	0.037	0.029	0.038	7.27E-06		
Green	MR	0.106	0.105	0.082	0.125	1.95E-04	–	1.48E-01
	H	0.115	0.125	0.082	0.136	3.70E-04		
Red	MR	0.205	0.191	0.175	0.262	8.51E-04	–	7.57E-04*
	H	0.246	0.255	0.216	0.275	4.82E-04		
NIR	MR	0.130	0.113	0.083	0.303	2.61E-03	3.99E-03*	–
	H	0.089	0.079	0.075	0.134	3.72E-04		
RedEdge	MR	0.199	0.197	0.153	0.316	1.41E-03	7.86E-01	–
	H	0.197	0.198	0.175	0.206	7.53E-05		
Metals (mg L^{-1})								
Total Li	MR	0.259	0.245	0.231	0.289	6.51E-04	–	6.35E-12*
	H	0.378	0.373	0.330	0.432	9.08E-04		
Total Mn	MR	1.167	1.118	1.053	1.285	9.31E-03	2.19E-23*	–
	H	1.918	1.919	1.885	1.946	3.09E-04		
Total Ni	MR	0.658	0.634	0.581	0.742	4.13E-03	4.33E-23*	–
	H	0.045	0.045	0.042	0.049	4.28E-06		
Total Pb	MR	0.297	0.279	0.260	0.333	8.70E-04	8.67E-22*	–
	H	0.067	0.067	0.064	0.072	6.54E-06		
Total S	MR	746.289	708.630	660.988	831.560	5.39E + 03	3.46E-14*	–
	H	477.994	477.558	473.786	485.357	1.11E + 01		
Total Zn	MR	4.115	4.110	3.556	4.580	1.39E-01	2.03E-24*	–
	H	0.025	0.023	0.020	0.036	3.45E-05		
Particulate Fe	MR	10.593	9.151	4.886	22.010	2.57E + 01	–	9.35E-01
	H	10.749	9.909	4.512	17.009	1.28E + 01		

Welch's *T*-test assuming unequal variance (W-T) and Tukey–Kramer (T-K) Test was used to assess significant differences between the two sets [e.g., Mayer Ranch Passive Treatment System (MR) and Hartshorne Passive Treatment System (H)] of samples; "–" in the T-K column indicates samples were analyzed using the W-T test, and vice versa both examinations were evaluated at p-value < 0.05, indicated by "*" for significantly different sets

the investigated metals, and Zn was only moderately related ($R = 0.64$, − 0.55, and 0.68) with Li, Mn, and Ni, respectively. However, the dominant OAC (e.g. particulate Fe) in this system displayed relationships of varying strength ($R = 0.83$, − 0.48, 0.71, − 0.54, 0.14, and 0.59) with Li, Mn, Ni, Pb, S, and Zn, respectively. Neither set of water quality data displayed significant signs of spatial autocorrelation (Moran's I) or hotspots (Getis-Ord Gi*). In total, outliers represented 10% (i.e. one water sample) and 7% (i.e. two water samples) of the data at HPTS and MRPTS, respectively. It appeared that both sets of outliers were produced while attempting to collect surface samples representative of reflectance measurements near surface debris (i.e. amorphous iron-oxyhydroxide) persistent in each oxidation pond.

Spectral Measurements

At MRPTS, an evaluation of the relationships between individual reflectance bands revealed strong relationships between blue and NIR ($R = 0.76$) and NIR and red-edge ($R = 0.76$). The red band exhibited relationships with the red-edge and green bands ($R = 0.68$ and 0.52, respectively). Otherwise, little to no correlation ($R < 0.50$) was observed for reflectance values at MRPTS sampling locations. Fortunately, issues with wind action (i.e. glint), cloud cover, and OD were minimal. However, interferences from surface debris (i.e. amorphous iron-oxyhydroxide) and algae growth were present, particularly in the southwestern and northeastern portions of the MRPTS oxidation pond, respectively (Fig. 1d).

Multispectral reflectance values at HPTS were more strongly correlated than MRPTS, but the most robust relationships were observed between the different sets of bands. The green band exhibited strong correlations with the red and NIR bands ($R = 0.92$ and -0.93, respectively). The red and NIR bands also displayed a strong negative relationship ($R = -0.78$). Surprisingly, little correlation between the red and red-edge bands ($R = 0.11$) existed. The lack of association between these bands could be due to some remote sensing interferences, even though all of the samples were collected outside of shade-affected areas. For example, the surface debris present at MRPTS was also present at HPTS but to a greater degree. On average, the red-edge band had a 25% greater response (i.e. higher reflectance) than the red band reflectance. Anderson and Robbins (1998) supported these results, finding that iron-oxyhydroxide precipitates have peak reflectance values above 700 nm where the center point (717 nm) of the red-edge band is positioned.

Furthermore, Jackisch et al. (2018) indicate that goethite has an absorption edge at 668 nm, which is the red band's center point, resulting in less reflectance. An evaluation of the hyperspectral profiles confirms the presence of this absorption feature in ODWs at both PTS (e.g. MRPTS 2 and 4 m, HPTS 2 and 3 m in Fig. 2). The absence of spectral outliers was confirmed using the remote sensing interference raster described above.

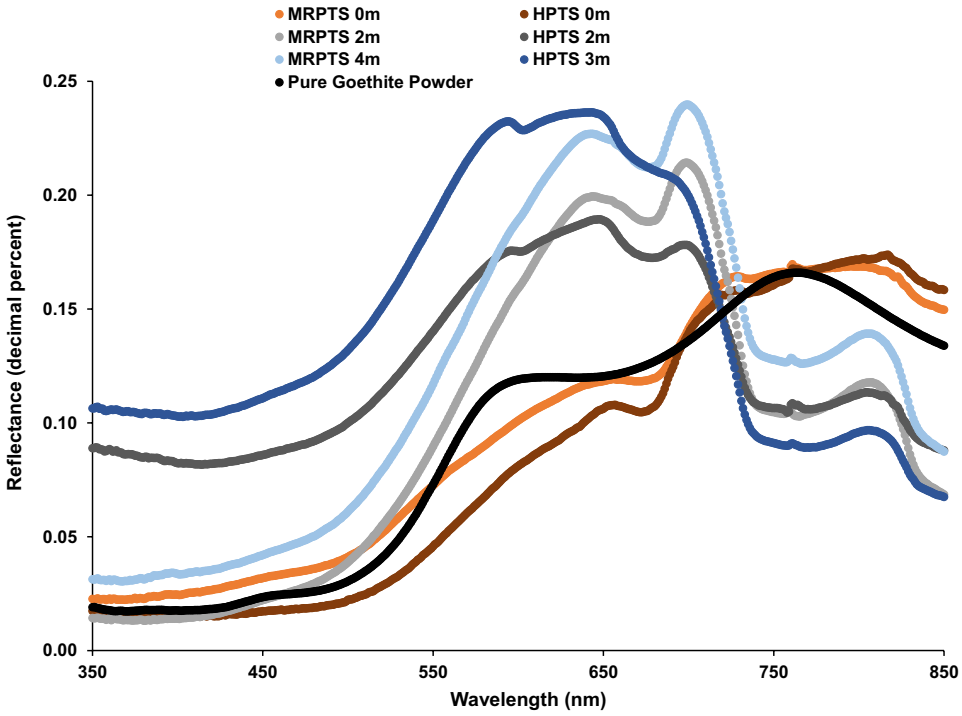

Fig. 2 Hyperspectral profiles displaying the effect that remotely sensing substrate (e.g. OSW) had on measured reflectance (e.g. MRPTS and HPTS 0 m) compared to ODWs (e.g. MRPTS 2 and 4 m; HPTS 2 and 3 m), with all compared to the reflectance of a sample of dried pure goethite powder from Kokaly et al. (2017)

Developing and Testing Surface Water Quality Models: MRPTS

Every explanatory variable (e.g. band or band ratio) included in each OLS regression model made significant contributions (p-value < 0.05). Each model was also statistically significant (p-value < 0.01; joint F statistic). The explanatory variables displayed no significant redundancy (VIF < 7.5), spatial autocorrelation (p-value > 0.05; global Moran's I), or clustering (p-value > 0.05; Getis-Ord Gi*) with one another. Values produced by the models displayed no significant bias (p-value > 0.01; Jarque–Bera statistic), and the residuals were not significantly different from a normal distribution. Overall, the Koenker statistic (p-value > 0.01) verified that the observed relationships were stationary and homoscedastic, indicating the models were properly specified (Table 3).

When tested at MRPTS, the assessed models (Table 4) produced promising results. All tests were performed on each sample and averaged to create a single value to simplify and more closely resemble the results of a traditional in-situ sampling event (i.e. one in-situ sample). Only three models (e.g. Fe, Ni, and S) produced a greater than 1% difference from the observed mean concentrations. The same models also exhibited the greatest bias at 0.64, 0.02, and 18.73 mg L^{-1}, respectively. Furthermore, only a 90% confidence interval for the Ni and S models could be achieved ([0.64, 0.66] and [718.45, 742.99], respectively). The standard deviation of the predicted Ni concentrations was the greatest for metals with mean concentrations below 1 mg L^{-1} (e.g. Li,

Table 3 Developed total and particulate metal models passing the set model criteria at MRPTS

Metal	Total Li	Total Mn	Total Ni	Total Pb	Total S	Total Zn	Particulate Fe
Coefficient 1	− 1.66	0.30	− 1.19	− 1.61	− 1508.99	− 4.267	110.48
Variable 1	G*	RE_G*	R*	G*	R*	R*	NIR*
Coefficient 2	0.21	− 0.98	− 0.23	0.11	− 282.67	− 0.71	− 5.81
Variable 2	B_NIR*	L_R*	NIR_R*	L_R_RE*	NIR_R*	NIR_G*	NIR_B**
Coefficient 3	0.094	− 0.62	0.19	0.11	225.18	1.39	24.49
Variable 3	L_B_RE*	L_R_NIR*	RE_G*	L_NIR_RE*	RE_G*	RE_G*	L_B_R**
Intercept	0.18	0.40	0.67	0.22	788.49	3.21	− 35.51
AICc	− 126.60	− 65.18	− 85.97	− 121.98	240.28	− 2.19	112.12
$R^2_{adjusted}$	0.76	0.76	0.77	0.78	0.76	0.74	0.81
Jarque–Bera p	0.99	0.97	0.67	0.98	0.70	0.70	0.74
Koenker p	0.17	0.42	0.63	0.26	0.34	0.99	0.05
Moran's I p	0.08	0.07	0.07	0.07	0.08	0.10	0.79
Getis-Ord p	0.84	0.86	0.77	0.96	0.90	0.70	0.24
Joint-F p	< 0.01	< 0.01	< 0.01	< 0.01	< 0.01	< 0.01	< 0.01
VIF	2.57	2.10	2.10	1.22	2.10	3.27	2.56

Blue, green, red, rededge, and NIR symbolized B, G, R, RE, and NIR, respectively. Log transformations of bands or band ratios abbreviated with "L". Significance at p-value (p) < 0.01 and 0.05 symbolized with * and **, respectively

Table 4 MRPTS testing metrics from developed OLS models passing set criteria

	Total Li	Total Mn	Total Ni	Total Pb	Total S	Total Zn	Particulate Fe
Measured mean	0.26	1.17	0.66	0.30	749.45	4.15	12.40
Predicted mean	0.26	1.17	0.65	0.30	730.72	4.14	11.76
Mean residual	− 3.45E-4	2.78E-3	1.58E-2	2.99E-4	1.87E + 1	1.34E-2	6.36E-1
MSE	0.00	0.07	0.01	0.00	10,523.59	0.01	12.13
MAE	0.01	3.24	0.03	0.01	18.73	0.17	3.61
Mean % difference	-0.13	0.24	2.39	0.10	2.50	0.32	5.13
Upper CL	0.27	1.18	0.66	0.30	745.96	4.20	12.75
Lower CL	0.26	1.15	0.63	0.29	715.48	4.10	10.78

All values presented in mg L^{-1}, unless otherwise noted [e.g., mean percent (%) difference]; Confidence limits (CL) for Li, Mn, Pb, Zn, and Fe were established at 70 percent while values for Ni and S represent the 90 percent confidence limit; MSE and MAE stand for Mean Standard Error and Mean Absolute Error, respectively

Ni, and Pb), increasing the relative size of the interval. As expected, Ni fell within the established confidence interval.

Regardless, the observed success of all of the other models (e.g. particulate Fe, and total Li, Mn, Pb, and Zn) warrant further discussion. These models displayed negative relationships ($R < -0.36$ and -0.58) with the blue and green bands, respectively, while exhibiting strong collinearity with each other ($R > 0.90$). Because the total metals were considered non-optical (i.e. constituents with little to no contribution to the observed spectra), the relationships with visible reflectance must be explained. The fact that the red band was not used more extensively to model the dominant optical parameter (i.e. particulate Fe) was somewhat unexpected. Theoretically, regions with deeper red colors would contain elevated particulate Fe concentrations and reflect proportionally more red EM energy. The observed strength ($R = 0.88$) of the linear relationship between the red band and particulate Fe supported this theory. Since the blue and green bands were included in every non-optical model, additional interactions must have occurred. Torrent and Baron (2002) note that Fe oxides can also reflect strongly in the NIR while absorbing blue energy. Therefore, as particulate Fe concentrations increased, so did the quantity of red EM reflected, which proportionally decreased the amount of blue and green EM reflected (i.e. spectral shifting). As concentrations of non-optical metals collinearly decreased, the amount of blue and green EM increased. However, due to the spectral shifting (i.e. dominant optical properties), the increase likely occurred at longer wavelengths (red, red-edge, or NIR). This shift was evident in the band or band ratios used to estimate the non-optical metals (a combination of blue, green, or NIR in every model).

Due to the novel nature of this study and lack of published literature on remotely estimating mine drainage metal concentrations, further discussion on relationships between non-optical metals and sUAS-derived reflectance is speculative. Even some of the most recent reviews (Dierssen et al. 2021) of spectral aquatic remote sensing fail to mention applications described in this study. Dierssen et al. (2021) do describe remote sensing science as being on the threshold of producing new techniques to describe aquatic ecosystems. New relationships and novel parameters, like those provided in this study, allow decision-makers and environmental monitors to make more informed choices. Thus, it appears this study exploited these fundamental EM interactions and physical relationships (e.g. prominence and adsorption capabilities of iron-oxyhydroxides) to successfully develop predictive, unbiased, and robust surface water quality models.

Although the 75% confidence interval of two models (e.g. Ni and S) did not contain the observed mean values, the overall success of the study warrants an acceptance of the first hypothesis. The observed mean values for only these two models were within all calculated confidence intervals above 85%. All other models had observed mean confidence level values of at least 70%. According to Petty (2012), a 95% confidence level is acceptable; however, some simulation experts use a confidence level of 80% for statistical validation. Therefore, the levels of confidence established were deemed appropriate for a novel environmental study of this nature.

Validating Surface Water Quality Models: HPTS

Validation of the models developed and tested at MRPTS at HPTS produced mixed results. Ideally, at each PTS, the relationships between the independent and dependent variables (i.e. in-situ water quality and multispectral reflectance, respectively) would be proportional. Unfortunately, that was not observed, either in terms of the band and band ratios used or the relationships' directionality. Otherwise, most models exhibited bias proportional to the differences in the two datasets' mean metal concentrations, and all concentrations, except Zn, produced randomly distributed residuals (Table 5 and Fig. 3).

The Zn model did not perform well because not only were the two water quality datasets significantly different

Table 5 HPTS validation metrics from applied OLS models developed at MRPTS

	Total Li	Total Mn	Total Ni	Total Pb	Total S	Total Zn	Particulate Fe
Measured mean	0.38	1.91	0.45	0.07	477.99	0.03	10.75
Predicted mean	0.29	1.23	0.67	0.10	790.09	4.04	10.21
Mean residual	0.09	0.68	− 0.22	− 0.03	− 312.09	− 4.01	0.54
MSE	0.07	4.69	0.42	0.01	876,610.00	144.79	2.60
MAE	0.09	0.76	0.22	0.03	312.09	4.01	1.55
Mean % difference	− 23.18	− 35.75	48.51	46.92	65.29	16,582.46	− 0.53
Upper CL	0.30	1.26	0.69	0.11	814.34	4.16	11.96
Lower CL	0.27	1.20	0.64	0.09	765.83	3.91	8.46

All values presented in mg L^{-1}, unless otherwise noted [e.g., e.g., mean percent (%) difference]. All established confidence limits (CL) represent the 95th percentile. MSE and MAE stand for Mean Standard Error and Mean Absolute Error, respectively

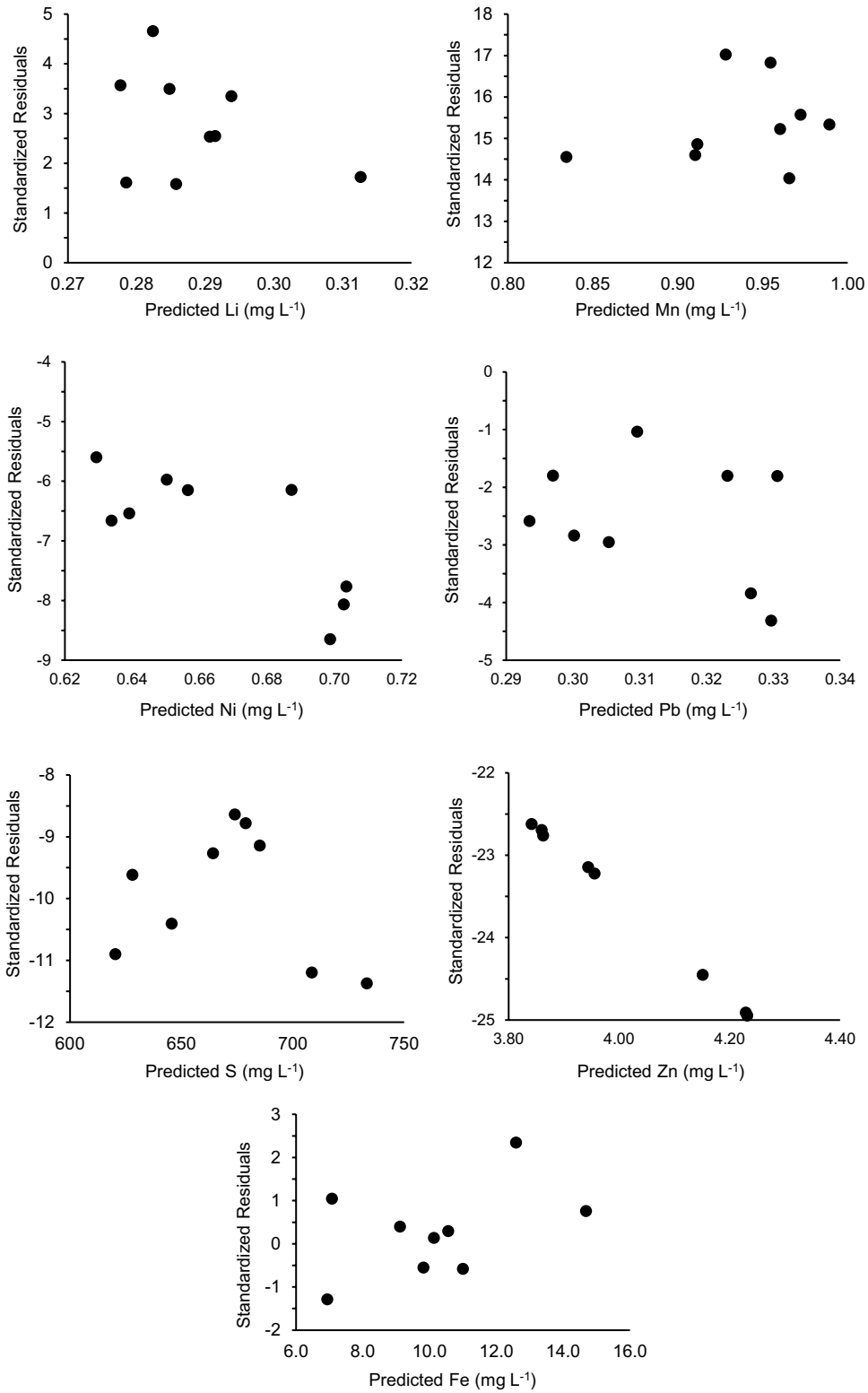

Fig. 3 HPTS OLS regression residuals normalized by the standard deviation of the population versus the examined metal concentration estimated by applying the MRPTS OLS models

(p-value = 2.03E-24; Welch's Test), but the difference was greater than two orders of magnitude. Reflectance measurements did not appear to be the cause because the bands (e.g. red and NIR) that exhibited significant differences (p-value < 0.05) between the two PTS were also used in some combination for all other models. These results suggest that the linear relationships developed at MRPTS were not capable of estimating the lesser concentrations

of Zn observed at HPTS. Since the color of the mine water at MRPTS and HPTS was comprised primarily by Fe, the ability to derive meaningful statistical relationships must be attributed to the prominence and adsorption capabilities of iron-oxyhydroxides.

The apparent need to develop site-specific IOPs (Salama et al. 2009) seems unnecessary and overly complicated, considering the disagreements regarding the theory of IOPs (Morel 2005). In-situ determinations of IOPs can prove problematic due to various physical, environmental, and instrumental limitations (Roesler and Boss 2007). Incorporating IOPs requires several assumptions, further complicating the modeling process, especially because it is impossible to measure the IOPs of each constituent (Roesler and Boss 2007). Thus, it appears that when remote sensing in the VIS/NIR range with limited spectral resolution (i.e. five narrow bands), sensor-perceived color had a greater impact. The color of the studied systems was primarily a result of reflectance from iron-oxyhydroxides within the water column. The optical prominence of Fe paired with its linear relationship with total Li ($R = 0.83$) allowed for the development of models capable of accurately (i.e. ± 25% of the measured value) describing these two metals (Table 4). However, in this study, the application of empirically derived surface water quality models confirmed the site-specific limitation discussed by numerous studies (Cannizzaro and Carder 2006; Gholizadeh et al. 2016; Lee and Carder 2002; Palmer et al. 2015; Salama et al. 2009; Su 2017; Voss et al. 2003). Although validation of meaningful statistical relationships was possible for two models (e.g. particulate Fe and total Li), all other models failed to meet the validation criteria (i.e. ± 25% of the measured value) (Table 4) and warrant further examination. Thus, the second hypothesis was rejected because five of the seven studied metal models were not verifiable within the criteria and scope of this study.

By completing several other analyses, it could be determined whether the hypothesis's rejection was due to the applied models or simply lack of relationships between variables. As mentioned earlier, the relationships between some of the independent and dependent variables at each PTS were drastically different. Exploratory regression was completed at HPTS to quantify these differences. This exercise resulted in an entirely different set of independent variables (e.g. band or band ratios) capable of effectively describing in-situ water quality at HPTS. All models were properly specified and homoscedastic (p-value > 0.01; Koenker statistic), produced statistically unbiased and normally distributed residuals (p-value > 0.01; Jarque–Bera statistic), and exhibited no evidence of spatial autocorrelation (p-value > 0.05; Moran's I; Table 6). The idea of using sUAS-derived multispectral imagery to model in-situ water quality appears to be statistically valid. Unsurprisingly, some data used to develop models tested at HPTS were significantly different (p-value < 0.05; Welch's Test and Tukey–Kramer) than values measured at HPTS (Table 2). The only variables that did not exhibit significant differences were the blue, green, and red-edge bands and particulate Fe concentrations (p-value = 0.07, 0.15, 0.79, and 0.94, respectively). Thus, the empirical nature of these models, particularly the range of OAC concentrations and types modeled paired with the difficulty of identifying relationships between various environmental processes across spatial and temporal scales, remains a complex challenge and requires future studies (Bennett et al. 2013; Dekker and Donze 1994; Seppelt et al. 2009).

Optical Depth Interferences

Detecting substrate through a water column decreased the overall EM reflected and, more importantly, altered the

Table 6 Results of exploratory regression analysis with models using only in-situ HPTS data that passed set criteria

	Total Li	Total Mn	Total Ni	Total Pb	Total S	Total Zn	Particulate Fe
Variable 1	+ R_NIR*	–	+ NIR*	+ G_NIR*	− B_R*	+ NIR*	− G_NIR*
Variable 2	+ RE_G*	− RE_R*	+ R_B*	+ RE_R*	− B_NIR*	+ G_NIR*	− NIR_B*
Variable 3	+ [Part. Fe]*	+ L_NIR*	− NIR_B*	− Turb**	+ L_B*	+ RE_R	+ Turb*
AICc	− 96.03	− 2.54	− 202.41	− 169.45	153.02	− 143.94	99.75
$R^2_{adjusted}$	0.99	0.90	0.99	0.80	0.99	0.77	0.96
Jarque–Bera p	0.11	0.10	0.45	0.93	0.23	0.57	0.12
Koenker p	0.14	0.21	0.12	0.16	0.27	0.03	0.16
Moran's I p	0.45	0.25	0.49	0.48	0.59	0.44	0.39
VIF	4.35	1.45	3.97	4.56	7.30	4.87	4.61

Blue, green, red, rededge, and NIR symbolized B, G, R, RE, and NIR, respectively. Particulate Fe concentrations and turbidity values symbolized as [Part. Fe] and Turb, respectively. Positive and negative signs before the variable indicate the directionality of the relationship. Significance at p-value (p) < 0.01 and 0.05 symbolized with * and **, respectively

overall spectral response (i.e. changes to peak reflectance wavelengths). Because it is impossible to separate individual OAC contributions to the response, some authors have used peak reflectance wavelengths to develop meaningful relationships (Anderson and Robbins 1998; Gholizadeh et al. 2016; Jackisch et al. 2018; Matthews and Odermatt 2015; Roesler and Boss 2007). Accounting for this issue often requires empirically derived models with numerous in-situ measurements (e.g. OAC concentrations, absorption coefficients, bottom depth, and bottom albedo) (Albert and Gege 2006; Cannizzaro and Carder 2006; Voss et al. 2003).

Instead, utilizing only sUAS-derived red band reflectance, in-situ measurements of SDD and AD, and the SDD to AD ratio, this study suggests a method to identify optically shallow or regions affected by other remote sensing interferences within ODWs. Using the SDD:AD ratio and red band reflectance at each PTS transect (OD model) produced a moderately strong negative exponential relationship ($R^2 = 0.73$) (Figs. 1d, f, and 6). The established exponential function (see equation in Fig. 4), modeled after the Beer-Lambert law, represented the decay of spectral energy in water. Considering that the OD model was developed from PTS with significantly different optical properties (e.g. red band reflectance), the agreement between the observed and predicted values, although small in sample size (n = 7), was encouraging (Fig. 5). It appears that the established methodology represents a reasonable approach to remotely evaluate a waterbody's potential for the application of sUAS technologies. Two spatial maps identifying the extent of remote sensing interferences (e.g. OSWs, algal blooms, surface debris, and shadows) demonstrate this application (Fig. 6a and b). Neither sUAS mission was void of remote sensing interferences. However, nearly all sampling locations were in areas unaffected by OD interferences (i.e. SDD: AD < 1.0). In future studies, optically complex waterbodies should first be evaluated with the OD model to assess the feasibility of employing remote sensing technologies for in-situ water quality monitoring.

Conclusions

Remote sensing with sUAS can produce accurate and reliable surface water quality models in ODWs with prominent optical properties. The exploitation of the natural (e.g. physical and chemical) relationships between various OACs allowed the development of non-optical metal models. When developed with PTS-specific reflectance and in-situ water quality, the results produced robust, unbiased, and accurate statistical models. Attempts to validate MRPTS models at HPTS suggest that the models were somewhat site-specific. However, further research will be required to determine whether the limitation resulted from the applied models, chemical and physical relationships (e.g. sorption) in the ponds, or significant differences between the test and validation datasets. A statistically derived exponential relationship represents a methodology to remotely assess the feasibility of utilizing the technologies described herein to assess ODWs. Currently, given the variability in accuracy, along with the lack of a standardized sUAS operating procedure

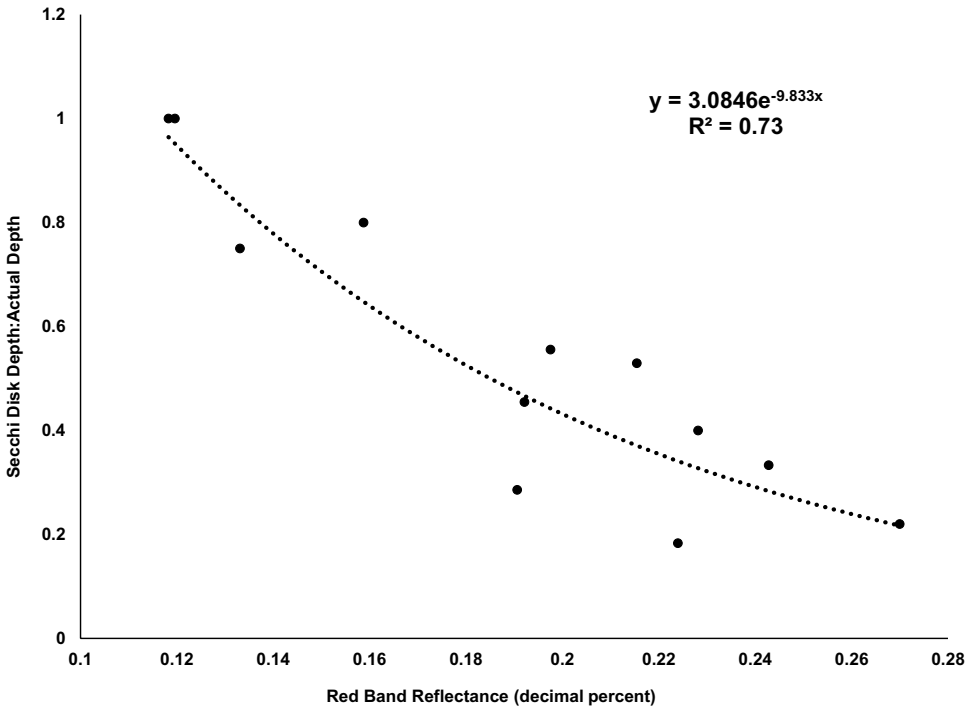

Fig. 4 Exponential relationship developed with data from both PTS to identify portions of ODWs impacted by optical depth (OD) and other remote sensing interferences

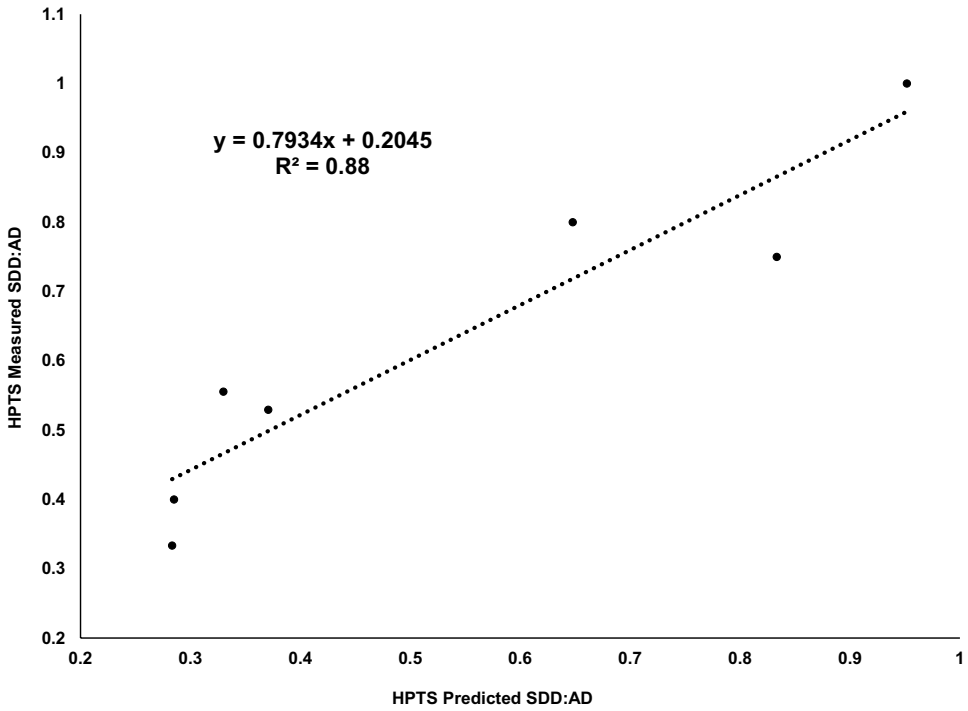

Fig. 5 Relationship between observed and predicted Secchi disk depth (SDD) actual depth (AD) ratio at HPTS

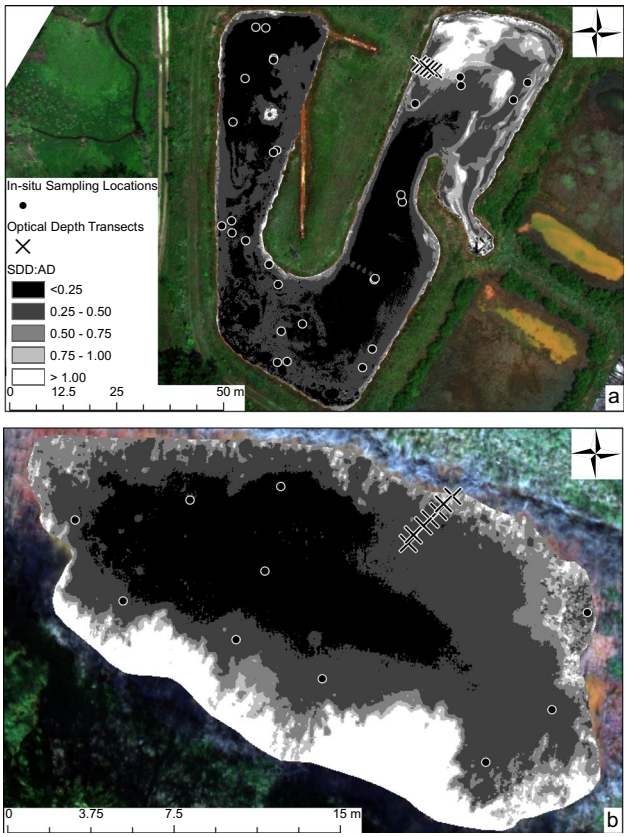

Fig. 6 Remote sensing interference (e.g., OSWs) surfaces within the study ponds at MRPTS (**a**) and HPTS (**b**) developed with in-situ spectral measurements at the marked transect locations and applied to the entire waterbody using the raster calculator in ArcMap V. 10.6.1

and reporting criteria, these technologies should only be used as exploratory tools. This study expands on the current OACs that can be estimated remotely and demonstrates the benefits of incorporating sUAS technologies into traditional mine water monitoring efforts. Ideally, in applications, these models will be continually refined, tested, and validated with surface water quality data from various types and forms of mine drainage systems. The systems and models discussed in this study may provide a reasonable alternative to in-situ surface water quality sampling and offer further insight into the nature of optically complex mine waters.

The methodology presented herein should be tested in ODWs dominated by an OAC with different optical properties (e.g. As, Cu, Pb, and Zn precipitates), on waters with lower OAC concentrations, and the commonly clear artesian source waters of mining-impacted environments. Alternative multispectral reflectance extraction techniques must be examined to determine which represent real-world conditions more accurately (Su and Chou 2015; Arango and Nairn 2020). If the goal is to minimize traditional in-situ sampling events and save time, money, and human hours, the widespread application requires that the models be refined with up-to-date water quality and reflectance measurements. Including data from each PTS in the model development phase could further refine and expand on the effective range of the models. Additional studies should be dedicated to understanding the effects of surface complexation with iron oxides on the sensitivity and validity of sUAS-derived surface water quality models.

Acknowledgements This work was supported by the Grand River Dam Authority (Agreements GRDA 060910 and GRDA 08272015). The authors appreciate the support from members of the Center for Restoration of Ecosystems and Watersheds (CREW), the additional spectral instrumentation provided by the Earth Observation and Modeling Facility (EOMF), and access to the property of private landowners.

References

Albert A, Gege P (2006) Inversion of irradiance and remote sensing reflectance in shallow water between 400 and 800 nm for calculations of water and bottom properties. J Appl Opt 45(10):2331–2343. https://doi.org/10.1364/ao.45.002331

Ali A, Strezov V, Davies P, Wright I (2017) Environmental impact of coal mining and coal seam gas production on surface water quality in the Sydney Basin Australia. J Environ Monit Assess 189(8):1–16. https://doi.org/10.1007/s10661-017-6110-4

Anderson J, Robbins E (1998) Spectral reflectance and detection of iron-oxide precipitates associated with acidic mine drainage. Photogramm Eng Remote 64(12):1201–1208

Arango J, Nairn R (2020) Prediction of optical and non-optical water quality parameters in oligotrophic and eutrophic aquatic systems using small unmanned aerial system. J Drones 4(1):1–21. https://doi.org/10.3390/drones4010001

Bebbington AJ, Humphreys Bebbington D, Sauls LA, Rogan J, Agrawal S, Gamboa C, Imhof A, Johnson K, Rosa H, Royo A, Toumbourou T, Verdum R (2018) Resource extraction and infrastructure threaten forest cover and community rights. Proc Natl Acad Sci 52:13164–13173

Becker RH, Sayers M, Dehm D, Shuchman R, Quintero K, Bosse K, Sawtell R (2019) Unmanned aerial system based spectroradiometer for monitoring harmful algal blooms: a new paradigm in water quality monitoring. J Great Lakes Res 45(3):444–453. https://doi.org/10.1016/j.jglr.2019.03.006

Bennett N, Croke B, Guariso G, Guillaume J, Hamilton S, Jakeman A, Marsili-Libelli S, Newham L, Norton J, Perrin C, Pierce S, Robson B, Seppelt R, Voinov A, Fath B, Andreassian V (2013) Characterizing performance of environmental models. J Environ Mod Soft 40:1–20. https://doi.org/10.1016/j.envsoft.2012.09.011

Biber E (2013) The challenge of collecting and using environmental monitoring data. J Ecol Soc 18(4):68. https://doi.org/10.5751/ES-06117-180468

Buczyńska A (2020) Remote sensing and GIS technologies in land reclamation and landscape planning processes on post-mining areas in the Polish and world literature. Proc Am Inst Phys Conf. https://doi.org/10.1063/5.0000009

Buters T, Bateman P, Robinson T, Belton D, Dixon K, Cross A (2019) Methodological ambiguity and inconsistency constrain unmanned aerial vehicles as a silver bullet for monitoring ecological restoration. Remote Sens 11(10):1180–1196. https://doi.org/10.3390/rs11101180

Cannizzaro J, Carder K (2006) Estimating chlorophyll a concentrations from remote-sensing reflectance in optically shallow waters. Remote Sens Environ 101(2006):13–24. https://doi.org/10.1016/j.rse.2005.12.002

Cress J, Hutt M, Sloan J, Bauer M, Feller M, Goplen S (2015) US geological survey unmanned aircraft systems (UAS) roadmap (2014). US Geol Sur Open-File Rep. https://doi.org/10.3133/ofr20151032

Dekker A, Donze M (1994) Imaging spectrometry as a research tool for inland water resources analysis. In: Hill J, Megier J (eds) Imaging spectrometry a tool for environmental observations, 4th vol. Springer, Dordrecht, pp 295–317

Dekker A, Zamurović-nenad Ž, Hoogenboom H, Peters M (1996) Remote sensing, ecological water quality modelling and in-situ measurements: a case study in shallow lakes. Hydrol Sci J 41(4):531–547. https://doi.org/10.1080/02626669609491524

Dierssen H, Ackleson S, Joyce K, Hestir E, Castagna A, Lavender S, McManus M (2021) Living up to the hype of hyperspectral aquatic remote sensing: science, resources and outlook. Front Environ Sci 9:649528. https://doi.org/10.3389/fenvs.2021.649528

ESRI (2018) Interpreting OLS results. Resource document ESRI. https://desktop.arcgis.com/en/arcmap/10.3/tools/spatial-statistics-toolbox/interpreting-ols-results.htm. Accessed 20 Dec 2020

Fang Y, Hu Z, Xu L, Wong A, Clausi D (2019) Estimation of iron concentration in soil of a mining area from UAV-based hyperspectral imagery. In: Proceedings 10th Workshop on Hyperspectral Imaging and Signal Processing: Evolution in Remote Sensing. Amsterdam, Netherlands, p 1–5

Federal Aviation Administration (FAA) (2016) Title 14: Aeronautics and Space | Part 107—small unmanned aircraft systems. FAA. https://www.ecfr.gov/cgi-bin/text-idx?SID=dc908fb739912b0e6dcb7d7d88cfe6a7&mc=true&node=pt14.2.107&rgn=div5#se14.2.107_13. Accessed 29 June 2020

Flores H, Lorenz S, Jackisch R, Tusa L, Contreras IC, Zimmermann R, Gloaguen R (2021) UAS-based hyperspectral environmental monitoring of acid mine drainage affected waters. Minerals 11(182):1–25. https://doi.org/10.3390/min11020182

Friedman S (1996) Map showing the distribution of underground mines in the Hartshorne and McAlester coals in the Hartshorne 7.5' quadrangle, Pittsburgh and Latimer counties, Oklahoma. U.S. Geological Survey Open-File Report 7–96.

Gholizadeh M, Melesse A, Reddi L (2016) A comprehensive review on water quality parameters estimation using remote sensing techniques. Sensors 16(8):1298–1340. https://doi.org/10.3390/s16081298

Holl K (2002) Long-term vegetation recovery on reclaimed coal surface mines in the eastern USA. J Appl Ecol 39(6):960–970. https://doi.org/10.1046/j.1365-2664.2002.00767.x

Holzbauer-Schweitzer B, Nairn R. (2020) Spectral monitoring techniques for optically deep mine waters. In: Pope J, Wolkersdorfer C, Sartz L, Weber A, Woldersdorfer K (eds), Proc, International Mine Water Assoc Congress, p 110–117

Jackisch R, Lorenz S, Zimmermann R, Möckel R, Gloaguen R (2018) Drone-borne hyperspectral monitoring of acid mine drainage: an example from the Sokolov lignite district. Remote Sens 10(3):1–23. https://doi.org/10.3390/rs10030385

Kokaly R, Clark R, Swayze G, Livo E, Hoefen T, Pearson N, Wise R, Benzel W, Lowers H, Driscol R, Klein A (2017) USGS spectral library version 7. USGS Data Ser. https://doi.org/10.3133/ds1035

LaBar J, Nairn R (2009) Evaluation of first 1.5 years of operation of a passive treatment system in SE Oklahoma. In: Barnhisel R (ed), Proc, National Meeting of the American Soc of Mining and Reclamation, p 693–708

Lee Z, Carder K (2002) Effect of spectral band numbers on the retrieval of water column and bottom properties from ocean color data. J Appl Opt 41(12):2191–2201. https://doi.org/10.1364/AO.41.002191

Lee S, Choi Y (2016) Reviews of unmanned aerial vehicle (drone) technology trends and its applications in the mining industry. Geosyst Eng 4:197–204. https://doi.org/10.1080/12269328.2016.1162115

Lee Z, Carder K, Mobley C, Steward R, Patch J (1998) Hyperspectral remote sensing for shallow waters—a semianalytical model. J Appl Opt 37(27):6329–6338. https://doi.org/10.1364/AO.37.006329

Lim J, Choi M (2015) Assessment of water quality based on Landsat 8 operational land imager associated with human activities in Korea. J Environ Monit Assess 187(6):4616. https://doi.org/10.1007/s10661-015-4616-1

Marquardt D (1970) Generalized inverses, ridge regression, biased linear estimation, and nonlinear estimation. Technometrics 12(3):591–612. https://doi.org/10.2307/1267205

Martins W, Lima M, Barros U Jr, Amorim S, Oliveira F, Schwartz G (2020) Ecological methods and indicators for recovering and monitoring ecosystems after mining: a global literature review. Ecol Eng. https://doi.org/10.1016/j.ecoleng.2019.105707

Matthews M, Odermatt D (2015) Improved algorithm for routine monitoring of cyanobacteria and eutrophication in inland and near-coastal waters. Remote Sens Environ 156:374–382. https://doi.org/10.1016/j.rse.2014.10.010

McKnight E, Fischer R (1970) Geology and ore deposits of the Picher field Oklahoma and Kansas. U.S. Geological Survey Professional Paper 588.

Morel A (2005) Introduction to optical properties of the sea: theoretical aspects. In: Babin M, Roesler C, Cullen J (eds) Real-time coastal observing systems for ecosystem dynamics and harmful algal blooms. UNESCO, Paris, pp 109–151

Nairn R, LaBar J, Strevett K, Strosnider W, Morris D, Garrido A, Neely C, Kauk K (2010) Initial evaluation of a large multi-cell passive treatment system for net-alkaline ferruginous lead-zinc mine waters. In: Barnhisel R (ed), Proc, 2010 National Meeting of the American Soc of Mining and Reclamation, p 635–649

Nairn R, LaBar J, Oxenford L, Shepherd N, Holzbauer-Schweitzer B, Arango J, Tang Z, Dorman D, Folz C, McCann J, Ingendorf JD, Stanfield H, Knox R. (2020) Toward sustainability of passive treatment in legacy mining watersheds: operational performance and system maintenance. In: Pope J, Wolkersdorfer C, Sartz L, Weber A, Woldersdorfer K (eds), Proc, International Mine Water Assoc Congress. p 123–128

ODEQ (Oklahoma Department of Environmental Quality) (2017) Tar Creek Superfund Site. Resource document ODEQ. https://www.deq.ok.gov/land-protection-division/cleanup-redevelopment/superfund/tar-creek-superfund-site/. Accessed 12 Nov 2020

Palmer S, Kutser T, Hunter P (2015) Remote sensing of inland waters: challenges, progress and future directions. Remote Sens Environ 157(2015):1–8. https://doi.org/10.1016/j.rse.2014.09.021

Park S, Choi Y (2020) Applications of unmanned aerial vehicles in mining from exploration to reclamation: a review. Minerals 10(663):1–31. https://doi.org/10.3390/min10080663

Petty M (2012) Calculating and using confidence intervals for model validation. Proc, Simulation Interoperability Workshop, p 10–14

Ren H, Zhao Y, Xiao W, Hu Z (2019) A review of UAV monitoring in mining areas: current status and future perspectives. Int J Coal Sci Technol 6(3):320–333. https://doi.org/10.1007/s40789-019-00264-5

Roesler C, Boss E (2007) In situ measurement of the inherent optical properties (IOPs) and potential for harmful algal bloom detection and coastal ecosystem observations. In: Babin M, Roesler C, Cullen J (eds) Real-time coastal observing systems for ecosystem dynamics and harmful algal blooms. UNESCO, Paris, pp 153–206

Salama M, Dekker A, Su Z, Mannaerts C, Verhoef W (2009) Deriving inherent optical properties and association inversion-uncertainties in the Dutch lakes. Hydrol Earth Sys Sci 13(7):1113–1121. https://doi.org/10.5194/hess-13-1113-2009

Seppelt R, Müller F, Schröder VM (2009) Challenges of simulating complex environmental systems at the landscape scale: A controversial dialogue between two cups of espresso. Ecol Model 220(24):3481–3498. https://doi.org/10.1016/j.ecolmodel.2009.09.009

Shi K, Zhang Y, Qin B, Zhou B (2019) Remote sensing of cyanobacterial blooms in inland waters: present knowledge and future challenges. Sci Bull 64(20):1540–1556. https://doi.org/10.1016/j.scib.2019.07.002

Su TC (2017) A study of a matching pixel by pixel (MPP) algorithm to establish an empirical model of water quality mapping, as based on unmanned aerial vehicle (UAV) images. Int J Appl Earth Obs Geoinfo 58(2017):213–224. https://doi.org/10.1016/j.jag.2017.02.011

Su TC, Chou HT (2015) Application of multispectral sensors carried on unmanned aerial vehicle (UAV) to tropic state mapping of small reservoirs: a case study of Tain-Pu Reservoir in Kinmen. Taiwan Remote Sens 7(8):10078–10097. https://doi.org/10.3390/rs70810078

Tiwari A, De Maio M (2018) Assessment of sulphate and iron contamination and seasonal variations in the water resources of a Damodar Vally coalfield, India: a case study. Bull Environ Cont Tox 100(2):271–279. https://doi.org/10.1007/s00128-017-2240-1

Torrent J, Barrón V (2002) Diffuse reflectance spectroscopy of iron oxides. Encycl Surf Colloid Sci (1):1438–1446. https://www.researchgate.net/publication/264869284_Diffuse_Reflectance_Spectroscopy_of_Iron_Oxides

Trumbull J (1957) Coal resources of Oklahoma. US Geol Sur Bull 1042:305–383

USGS (United States Geological Survey) (1996) 1995 national oil and gas assessment plays and 1995 national oil and gas assessment ¼-mile cells within the 6200 Arkoma Basin Province. USGS Central Energy Resources Team. https://certmapper.cr.usgs.gov/data/noga95/prov62/spatial/doc/prov62.xml. Accessed 10 Jan 2021

Voss K, Mobley C, Sundman L, Ivey J, Mazel C (2003) The spectral upwelling radiance distribution in optically shallow waters. Limnol Oceanogr 48(1):364–373. https://doi.org/10.4319/lo.2003.48.1_part_2.0364

Watts A, Ambrosia V, Hinkley E (2012) Unmanned aircraft system in remote sensing and scientific research: classification and considerations of use. Remote Sens 4(6):1671–1692. https://doi.org/10.3390/rs4061671

Werner T, Mudd G, Schipper A, Huijbregts M, Taneja L, Northey S (2020) Global-scale remote sensing of mine areas and analysis factors explaining their extent. Glob Environ Change 60(2020):1–10. https://doi.org/10.1016/j.gloenvcha.2019.102007

Whitehead K, Hugenholtz C (2014) Remote sensing of the environment with small unmanned aircraft systems (UASs), part 1: a review of progress and challenges. J Unmanned Veh Syst 2(3):69–85. https://doi.org/10.1139/juvs-2014-0006

Zeng C, Richardson M, King D (2017) The impacts of environmental variables on water reflectance measured using a lightweight unmanned aerial vehicle (UAV)-based spectrometer system. J Photogram Remote Sens 130:217–230. https://doi.org/10.1016/j.isprsjprs.2017.06.004

Zhang Z, Li H, Cybele M, Dai W, Li Z (2019) Remotely sensed water reflectance measurements based on unmanned aerial vehicle (UAV). In: Chung J, Triantafyllou M, Langen I, Yao T (eds), Proc, 29th International Ocean and Polar Engineering Conf, p 614–619